Microhole-pair hollow core fiber Fabry–Perot interferometer micromachining by a femtosecond laser

Cheng-Ling Lee [a],[*], Yang Lu [a], Chien-Hsing Chen [b], Chao-Tsung Ma [c]

[a] Department of Electro-Optical Engineering, National United University, Miaoli, 360, Taiwan
[b] Department of Biomechatronics Engineering and General Research Service Center, National Pingtung University of Science and Technology, Pingtung, 912, Taiwan
[c] Department of Electrical Engineering, National United University, Miaoli, 360, Taiwan

A B S T R A C T

This study presents a sensitive and high-response microhole-pair (MP) hollow-core fiber (HCF) Fabry–Perot (FP) interferometer (MPHCFFPI) by microdrilling two holes symmetrically on the sidewall of the HCF via a femtosecond laser micromachining technique. The dimension of FP microcavity in the MPHCFFPI is length of the HCF. Only 0.005 s is needed to completely fill the HCF cavity with alcohol via the capillary action of the MP. The MPHCFFPI is developed to measure the thermo-optic coefficients (TOCs) and refractive indices (RIs) of liquids to investigate its effectiveness and accuracy. The TOCs of the deionized water, ethanol, and acetone are accurately determined as -1.076×10^{-4}, -3.11×10^{-4}, and $-4.28\times10^{-4}\,^{\circ}C^{-1}$, respectively. The measured RIs of liquids ranging from 1.3 to 1.6 also highlight that the proposed fiber sensor can achieve higher RI than the silica fibers.

© 2019 Elsevier B.V. All rights reserved.

1. Introduction

Ultrafast laser processing with femtosecond (fs) lasers can be used for the most challenging tasks, especially for fabricating high-precision holes and lines without thermal damage. Various micro or nanoscale machining techniques have been accomplished by fs lasers to process advanced devices and materials. These techniques are urgent and practical for the industry and technology because fs laser processing can be performed for microdrilling, writing, and cutting materials, such as metals, ceramics, polymers, and dielectrics. For fiber optic applications, many fiber Fabry–Perot interferometers (FFPIs) and fiber Mach-Zehnder interferometers (FMZIs) have been fabricated by using fs laser micromachining (FSLM) to achieve ultracompact and precise performance [1–12]. Precise material ablation can be realized with extremely high peak power with minimized heat-affected zone, controlled cavity length, and fast fabrication. Thus, many studies have been conducted on the opening of micro-notch cavity on single-mode fibers (SMFs) and photonic crystal fibers (PCFs) fabricated by FSLM [1–6]. In 2007, Y. J. Rao et al. reported the novel demonstration of the direct machining of a micro-FPI on an SMF and a PCF with a microrectangular notch

structure by using fs laser [1]. Direct FSLM has been used to precisely fabricate air-gap microcavities on fibers to form FFPIs [2–5] and FMZIs [6,7] for high sensing configurations. Here, the FPIs are the most fabricated with a micronotch or a microchannel by fs laser, and the MZIs are created by removing part of the fiber core near the core and cladding interface by fs laser. The advanced FSLM can accurately control the microhole length and micronotch depth on the fibers. However, such direct micromachining by fs laser ablation results in non-parallel walls of the microcavity/microhole, rough surface of the cavity, and poor mechanical strength. In addition, the micromachining process by removing the material layer-by-layer is time consuming with certain complications. To overcome these issues, a new method for making a smooth inner surface of the air cavity is fabricated by FSLM combined with fusion splicing technique [8–11]. A microhole is first drilled into the cleaved end face of an SMF by fs laser. The hole-drilled SMF is then spliced to another SMF to form an air cavity between the two fibers. After the fusion splicing, the rough walls of the cavity are melted by the arc, and a much smoother structure is obtained. The above studied sensors can achieve a smoother reflection surface. However, the aspect ratio of the laser beam drilling still results in the fabrication of non-parallel walls (sphere surfaces) of the cavity/hole. It should be noted that, C. R. Liao et al. have further inscribed a micro-channel vertically cross the above mentioned cavity by fs laser micromachining to allow the measured liquids to flow into

* Corresponding author.
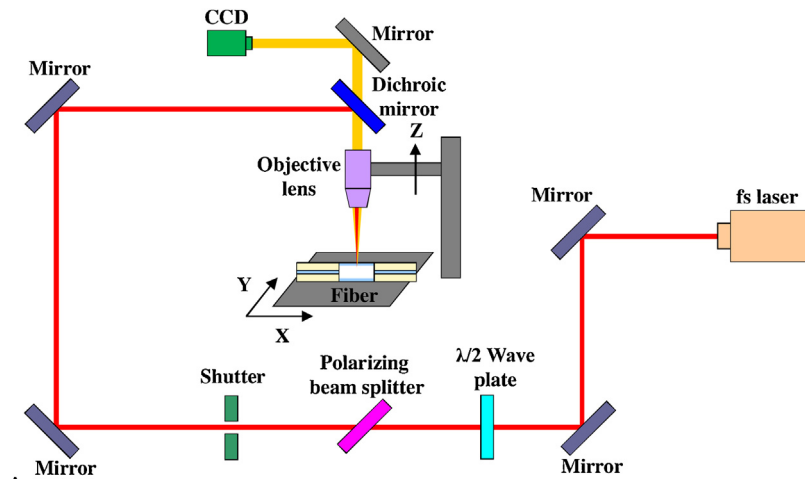 *E-mail address:* cherry@nuu.edu.tw (C.-L. Lee).

Fig. 1. Schematic of the fs laser machining system.

the cavity for RI sensing [9]. The approach is novel and very effective for measuring the parameters of liquids, however the reflected light beam from hollow sphere surfaces with large curvature would be divergent, which leads to an extremely poor fringe visibility of the corresponding fringe patterns [9]. To overcome this problem, we first demonstrate a microhole-pair (MP) hollow-core fiber (HCF) Fabry–Perot interferometer (MHCFFPI) by symmetrically drilling two microholes on the sidewall of the HCF by FSLM. The FP microcavity is obtained only by fusion splicing a tiny section of the HCF between two SMFs. The length of the FP cavity is fixed by the HCF section, and the cavity walls are the endfaces of the fused SMFs that are flat and parallel. The proposed approach can completely solve the problem of non-parallel mirrors in the FP cavity by FSLM. Then, the surface of the HCF is straightly pierced with microholes through the claddings of HCF by FSLM. Y. P. Wang et al. presented the fs laser microdrilling of a hole on an HCF to fabricate a gas pressure sensor [12]. However, their study is not focused on the flat and smooth-processed surfaces of FP cavity. The microhole is only used to diffuse the gas into the HCF core, and the HCF cladding functions as an antiresonant reflecting guidance waveguide. Based on our experience, fully filling gases or liquids into the HCF via a single microhole takes a considerable amount of time. By contrast, the duration of capillary action to fully fill liquids into the HCF with the proposed microhole pair only takes 0.005 s to investigate the high response and effectiveness of the sensor. Thus, the proposed configuration with such a miniature FP cavity is effective and can be applied to measure several physical and optical parameters of microspecimens of liquids or gases.

2. Sensor fabrication

The studied device is initially based on an HCF FP interferometer, which is only made by two SMFs and a tiny section of an HCF with diameter of D = 75 μm. The HCF interferometer is fabricated by fusion splicing a section of the HCF (length of about L = 50 μm) between two flat cleaved SMFs. After the splicing of the HCF, the end face of SMF is cleaved with a slant to prevent the undesired Fresnel reflection from the fiber/air interface. Then, a section of the HCF is processed by fs fiber laser machining. The HCFs are mainly composed of fused silica, which are hard, fragile, and have a band gap energy of 9 eV. These characteristics may induce microcracks or heat-affected zones when machined with long pulsed lasers. The fs laser has an ultra-short pulse duration and very strong peak power intensity that can induce nonlinear multiphoton absorption to enable the photo-ionization and avalanche ionization of a mate-
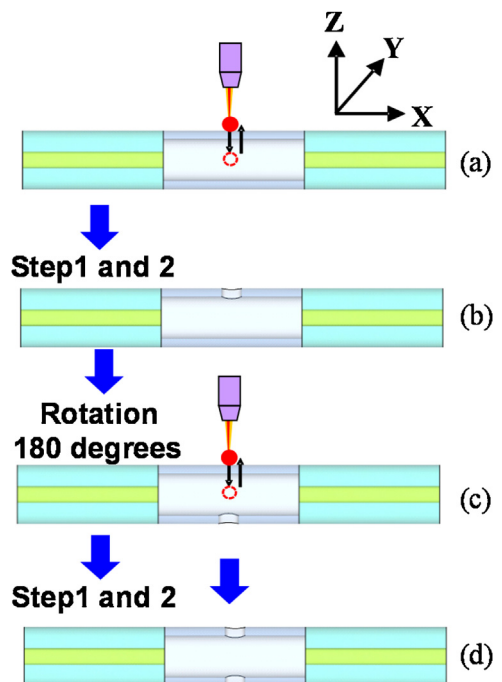

Fig. 2. Main steps in the formation of the hole–pair structure of the optical fiber interferometer by fs laser machining system.

rial during fs laser irradiation. Given the nonlinear multiphoton absorption, the fs laser can be used to precisely engrave optical fibers.

The fs fiber laser machining system (Light Conversion, Model CB5-85) in this study is shown in Fig. 1. The central wavelength of the laser is 1028 nm ± 5 nm, the pulse duration is less than 400 fs, and the repetition rate is 1 MHz. The laser beam is a Gaussian beam. In the machining process, the proposed HCF interferometer is placed on the X-Y micropositioning platform. The laser power is tuned by rotating the half-wavelength and polarization slides. The laser beam spot is focused by a 10× objective lens (Mitutoyo, Model M Plan Apo NIR) mounted on a Z stage. The fiber device is fastened by a clamping apparatus. The machining path and rate are controlled by programming the X-Y micro-positioning platform. An optical microscope is used to examine the machined products. The fabrication process is monitored in situ by a charge-coupled device.
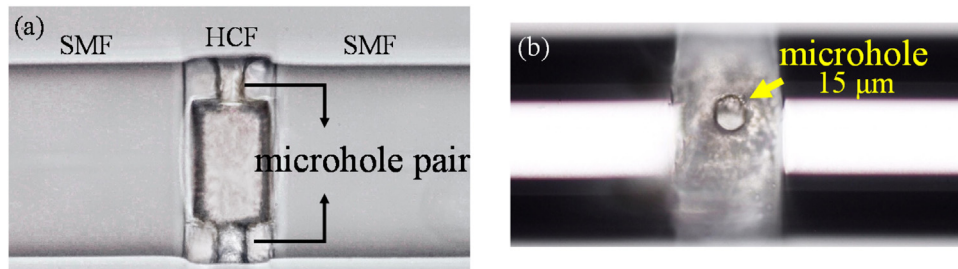
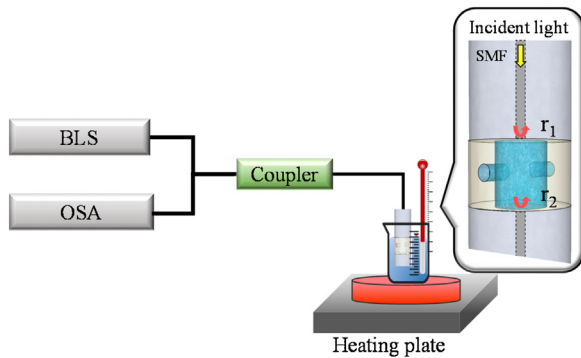**Fig. 3.** Micrographs of (a) the sensor with two drilled microholes and (b) the microhole on the HCF surface.

Fig. 4. Schematic diagram of the experiment setup.

Fig. 5. Spectra before and after laser micromachining.

The fs laser, with an average power of 2 W and focal spot size of about 20 μm, is focused on a spot on the surface of the HCF. The scanning length (along the z-axis) and speed are 60 μm and 0.01 mm/s, respectively. The following are the steps to form the MP structure on the fiber interferometer. In step 1, the laser is turned off, and the focal height is adjusted to the surface of the HCF, $z = 0$ (Fig. 2a). In step 2, the fs laser source is turned on, and a scan is performed by sweeping the defined scanning length in the HCF from top to bottom along the z-axis with the stated scanning speed. As a result, a microhole is drilled on the cladding of the HCF, as illustrated in Fig. 2(b). To fabricate another microhole in the symmetrical side of the cylindrical HCF, the HCF device is rotated by 180°, as displayed in Fig. 2(c). Then, steps 1 and 2 are repeated until two microholes are obtained (Fig. 2d). Fig. 3(a) and (b) are the micrographs of the fabricated sensor with the MP and top view of the HCF surface, repectively.

After the sensor has been fabricated, the microholes are filled with liquids by immersing the sensor into the liquids. Fig. 4 depicts the experimental setup to measure the liquids. When a broadband light source (BLS) is propagated to the device, the two reflective beams from the r_1 and r_2 interfaces are combined and returned to the SMF to produce interference patterns. Variations in the interference spectra with the parameters of the liquids are readily monitored and analyzed using an optical spectrum analyzer (OSA).

3. Experimental result and discussion

Fig. 5 illustrates that the proposed MPHCFFPI can achieve high extinction ratio (approximately 15 dB) in the fiber FP interference. The results also demonstrate that the optical interference spectra of the device are very similar before and after laser micromachining. This finding verifies the stability of the FP microcavity, and the drilling of microholes by the fs laser cannot affect the HCF cavity. When the microcavity is immersed into liquids filled with deionized (DI) water to test the effectiveness of the microcavity, HCF with the two microholes can be quickly filled with water, and its optical spectrum does not change immediately.
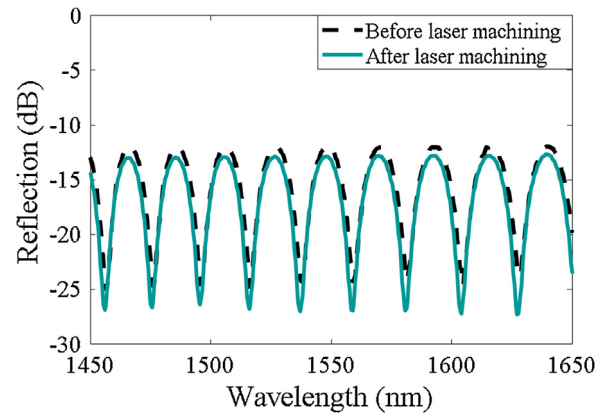
To evaluate the duration of capillary action, a laser diode (LD) with wavelength of 1544 nm that is launched into the sensor and its response can be detected and analyzed by a photodecector and an oscilloscope. The duration of sidewall capillary action by the microhole pair only takes respectively 3.12 and 0.005 s for water and alcohol that is much shorter than that by one microhole on the HCF, as shown in the Fig. 6(a) and (b). Based on our previous experiment, it took much more time to fully fill liquids into the HCF by one microhole condition (yellow line) [13]. As can be seen the results in the Fig. 6, water with highly polar molecules would have high cohesion to make high surface tension. It would make water not easy to fill into the cavity through the microholes. However, the alcohol with very high volatility would achieve much shorter response time.

The proposed sensor can measure different kinds of liquids with high effectiveness. The temperature (T) of the liquids can be changed to evaluate the opto-thermal effects and determine the thermo-optic coefficients (TOCs) of the liquids. In the TOC measurement, the T of the liquids is increased from 25 °C to 55 °C, with a step increment of 1 °C. The interference spectra of the sensor shift to short wavelengths to illustrate the decrease in the refractive index (RI) of the liquid. The fiber sensor must be rinsed with 99.99 % pure alcohol after each measurement. The pure alcohol with very high volatility can remove the residual liquids effectively. Fig. 7(a)–(c) display the detailed shift in the wavelength ($\Delta\lambda$) of the interference peaks as T increases because of the thermal effect on the liquids, namely, DI water, alcohol, and acetone. The wavelength is blue-shifted, and the peak intensity is slightly increased as the RI decreases with increasing T. These phenomena result in the enhancement of the Fresnel reflection. The measured sensitivities ($\Delta\lambda/\Delta T$) are negative and highly linear from 25 °C to 55 °C in the three cases. These results indicate that the TOC values of these materials are almost stable during the range of measured T. The experimental results also indicate that a large slope of $\Delta\lambda$ as a function of T corresponds to a high estimated TOC.
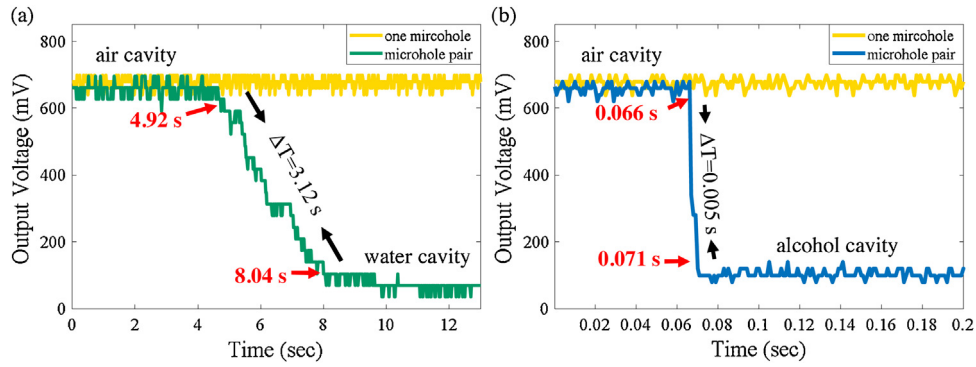
Fig. 6. Dynamic responses of filling different liquids through the microhole pair for (a) water and (b) alcohol.
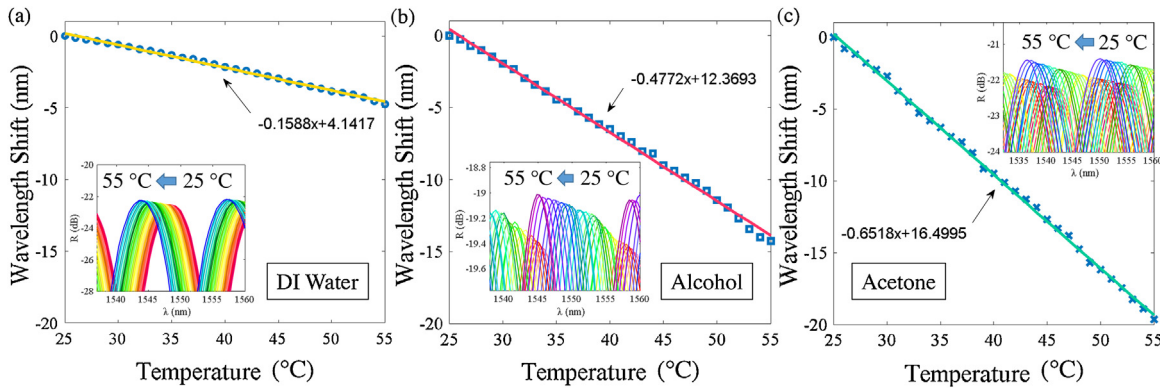

Fig. 7. Optical spectra and $\Delta\lambda$ sensitivities of the sensor from 25 °C to 55 °C for (a) water, (b) alcohol, and (c) acetone.

Based on the experimental results in Fig. 7, the TOC of the test liquids can be calculated by analyzing the $\Delta\lambda$ in the interference peaks [14]. The TOC can be calculated as follows:

$$\text{TOC}(\lambda) = \frac{\frac{\lambda'}{\lambda} - \alpha\Delta T - 1}{\Delta T + \alpha\Delta T^2} \quad (1)$$

where α is the thermal expansion coefficient of silica fiber ($\sim 5.5 \times 10^{-6}$ °C^{-1}), and $\Delta\lambda$ is the shift in the interference peak defined as the shifting of wavelength λ to λ' when T changes to T'. The latter indicates that λ and λ' correspond to the interference peaks at T and $T'= T+\Delta T$, respectively. Eq. (1) indicates that the measured TOCs are slightly correlated with operator λ. Here, the determined TOCs of the DI water, alcohol, and acetone at approximately $\lambda = 1550$ nm are -1.076×10^{-4} °C^{-1}, -3.11×10^{-4} °C^{-1}, and -4.28×10^{-4} °C^{-1}, respectively. The results closely agree to previously reported values [14–17], as shown in Table 1.

To determine the RIs (n_D) of the materials, the sensor head is immersed in a series of standard RI liquids from @Cargille Lab. The RIs of the liquids are in the range of $n_D = 1.3$–1.6. Here n_D is the RI value measured at 25 °C, sodium D line, 589.3 nm. Many studies have shown that the RI sensing based on the silica fibers are valid only in the guided configuration [18,19]. That is, the external n_D is lower than that of silica at approximately 1.46. The case of an external index higher than that of the silica fibers shows a leaky configuration, which is nonsensitive to high n_D greater than the RI of the fiber (denoted as n_f). To conceive a further sensitive fiber sensor operating in a leaky configuration, an in-fiber MZI based on the composed two 3 dB long-period gratings (LPGs) is used to sense external RI higher than those of silica fibers [20]. Fig. 8(a) shows the reflection spectra corresponding to the n_D from 1.3 to 1.6, which illustrates the extremely high sensitivity of the sensor. The fringe visibilities (FVs) decrease as n_D increases from 1.3 to approximately 1.44 and increase as n_D increases from 1.47 to

1.6. Good linear responses are observed with different n_D values ranging from 1.3 to 1.45 and from 1.47 to 1.6, with determined sensitivities of -53.62 dB/RIU and $+46.47$ dB/RIU, respectively. Given the index matching in region II, interference patterns almost vanish at approximately $n_D = 1.45$–1.47.

To analyze the characteristics of the measured reflection of the interference spectra in the Fourier domain, we analyze the optical spectral information in Fig. 8(a) by fast Fourier transform (FFT). We also obtain the spatial frequency spectra, as presented in Fig. 9(a), which exhibits the variations in the Fourier spectra corresponding to the n_D values. The peak intensity is also highly decreasing as n_D increases until $n_D = 1.46$ and increases as n_D increases to 1.6, as displayed in Fig. 9(b). Monitoring the amplitude of the autocorrelation peak is efficient to measure the n_D values. The analytical results of the Fourier spectral domain can also show that n_D is higher or lower than that of the silicas by the location of the spatial frequency of the resonances. The spatial frequency redshift of the materials with high n_D can be ascribed by the long optical path difference in the FP cavity with a slightly high optical phase. The periodicity of the spectral fringes of the interference spectra can be expressed using the free spectral range (FSR), FSR $\cong \lambda_2 - \lambda_1$ as follows:

$$\text{FSR} = \frac{\lambda_1\lambda_2}{2n_D L}, \quad (2)$$

where λ_2 and λ_1 are the wavelengths of two adjacent peaks in the interference spectrum; L is the cavity length, and n_D denotes the RI of the liquid filling cavity. Here, spatial frequency f_s can be simply expressed as follows:

$$f_s = \frac{1}{\text{FSR}} \quad (3)$$

Based on Eq. (2), the cavity filled with liquids with large n_D values can have small FSRs that cause large spatial frequency f_s. Thus,

Table 1
Comparisons of measured TOCs of the used liquids.

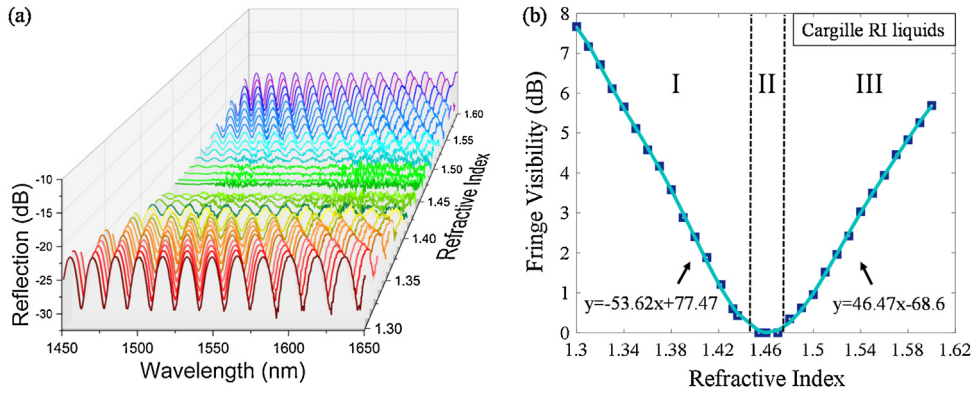| Liquids	DI Water	Alcohol	Acetone
TOC : K $[°^{-1}]$ at 1550 nm (measured in the study)	-1.076×10^{-4}	-3.11×10^{-4}	-4.28×10^{-4}
TOC : K $[°^{-1}]$ at 1550 nm (reference data)	-7.657×10^{-5} [14] -1.128×10^{-4} [15] -8×10^{-5} [17]	-3.688×10^{-4} [14] -3.117×10^{-4} [15] -3.99×10^{-4} [17]	-5.0747×10^{-4} [16]

Fig. 8. (a) Reflection spectrum for $n_D = 1.3-1.6$ and (b) Fringe visibility versus RI value.
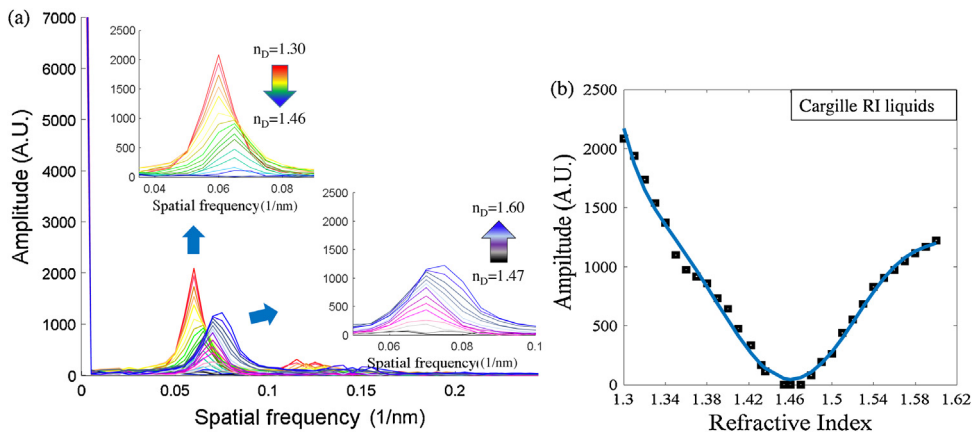

Fig. 9. (a) Spectra of the spatial frequency of the Fourier domain from $n_D = 1.3-1.46$ and (b) the amplitude responses versus RIs.
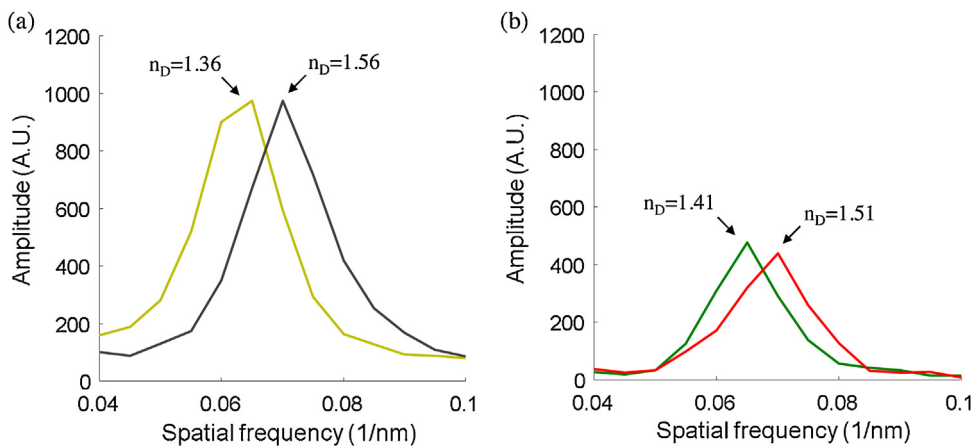

Fig. 10. Spatial frequency spectra with the same signal amplitude for (a) low $n_D = 1.36$ and high $n_D = 1.56$ and (b) low $n_D = 1.41$ and high $n_D = 1.51$.

the spectra of the spatial frequency with the almost same amplitudes are observed at n_D = 1.36 (n_D < n_f), and n_D = 1.56 (n_D > n_f). However, these spectra can be well distinguished from those of the spatial frequency of the Fourier domain (Fig. 10). The wide range of measured n_D of the liquids from 1.3 to 1.6 can be demonstrated by the proposed fiber sensor, especially achieving the measurement of RI values higher than that of the silica fibers.

4. Conclusion

An MPHCFFPI has been proposed and demonstrated for the rapid and precise measurement of TOCs and RIs. The MPHCFFPI is formed with a liquid-filled HCF and two microholes drilled through the cavity of the HCF by an fs laser for fast capillary action. The duration of sidewall capillary action by the microhole pair only takes respectively 3.12 and 0.005 s for water and alcohol that is much shorter than that by one microhole on the HCF and demostrates the advantages of the sensing configuration. The effectiveness of the fs laser microstructuring on the HCF is verified, and the feasibility of capillary action by microhole pair on the HCF sidewall is demonstrated. The proposed MPHCFFPI can be used for the fast and accurate determination of the TOC and the RI values of gases/liquids with picoliter volume. The wide range of measured RI values of the liquids from 1.3 to 1.6 has been demonstrated, especially achieving the measurement of RI values higher than that of the silica fibers. We believe that the ultracompact in-line fiber optic sensor with high response is very suitable to measure the other parameters of micro-specimens in the biomedical and biochemical fields.

Author contributions

This work was carried out in collaboration between all authors. The first author Chen-Ling Lee led on the study, performed the results analysis and wrote the first draft of the manuscript. Authors, Yang Lu, the master student in the Department of Electro-Optical Engineering, NUU, performed the experiments, managed data and figures. The author, Chien-Hsing Chen, from Department of Biomechatronics Engineering, NPUST, performed the experiments of fs laser micromachining. The last author, Chao-Tsung Ma, evaluated the sensing method, arranged the laser driving devices and provided discussions in preparation of the paper.

Declaration of Competing Interest

The authors declare that they have no known competing financial interests or personal relationships that could have appeared to influence the work reported in this paper.

Acknowledgement

References

[1] Y.J. Rao, M. Deng, D.W. Duan, X.C. Yang, T. Zhu, G.H. Cheng, Micro Fabry-Perot interferometers in silica fibers machined by femtosecond laser, Opt. Express 15 (21) (2007) 14123–14128.

[2] T. Wei, Y. Han, Y. Li, H.L. Tsai, H. Xiao, Temperature-insensitive miniaturized fiber inline Fabry-Perot interferometer for highly sensitive refractive index measurement, Opt. Express 16 (8) (2008) 5764–5769.

[3] T. Wei, Y. Han, Y. Li, H.L. Tsai, H. Xiao, Miniaturized fiber inline Fabry–Perot interferometer fabricated with a femtosecond laser, Opt. Lett. 33 (6) (2008) 536–538.

[4] Y. Liu, S. Qu, Y. Li, Single microchannel high-temperature fiber sensor by femtosecond laser-induced water breakdown, Opt. Express 38 (3) (2013) 335–337.

[5] P. Chen, Y. Dai, D. Zhang, A novel FPI sensor for high temperature sensing by femtosecond laser, 26th International Conference on Optical Fiber Sensors (2018) WF93.

[6] Y. Wang, M. Yang, D.N. Wang, S. Liu, P. Lu, Fiber in-line Mach–Zehnder interferometer fabricated by femtosecond laser micromachining for refractive index measurement with high sensitivity, J. Opt. Soc. Am. B 27 (3) (2010) 370–374.

[7] M. Janik, A.K. Mysliwiec, M. Koba, A. Celebanska, W.J. Bock, Sensitivity pattern of femtosecond laser micromachined and plasma-processed in-fiber Mach-Zehnder interferometers, as applied to small-scale refractive index sensing, IEEE Sens. J. 17 (11) (2017) 3316–3322.

[8] Y. Ran, Y. Rao, J. Zhang, Z. Liu, B. Xu, A miniature fiber-optic refractive-index sensor based on laser-machined Fabry–Perot interferometer tip, J. Lightwave Technol. 27 (23) (2009) 5426–5429.

[9] C.R. Liao, T.Y. Hu, D.N. Wang, Optical fiber Fabry-Perot interferometer cavity fabricated by femtosecond laser micromachining and fusion splicing for refractive index sensing, Opt. Express 20 (20) (2012) 22813–22818.

[10] Y. Zhang, L. Yuan, X. Lan, A. Kaur, J. Huang, H. Xiao, High-temperature fiber-optic Fabry–Perot interferometric pressure sensor fabricated by femtosecond laser, Opt. Lett. 38 (22) (2013) 4609–4612.

[11] W.W. Li, D.N. Wang, Z.K. Wang, B. Xu, Fiber in-line Mach–Zehnder interferometer based on an inner air-cavity for high-pressure sensing, Opt. Express 26 (9) (2018) 11496–11502.

[12] M. Hou, F. Zhu, Y. Wang, Y. Wang, C. Liao, S. Liu, P. Lu, Antiresonant reflecting guidance mechanism in hollow-core fiber for gas pressure sensing, Opt. Express 24 (24) (2016) 27890–27898.

[13] Y. Lu, C.H. Chen, C.T. Ma, C.L. Lee, A hollow core fiber Fabry–Perot interferometer micromachining by femtosecond laser, 24th Optoelectronics and Communications Conference (2019), 8817899.

[14] C.L. Lee, H.Y. Ho, J.H. Gu, T.Y. Yeh, C.H. Tseng, Dual hollow core fiber-based Fabry–Perot interferometer for measuring the thermo-optic coefficients of liquids, Opt. Lett. 40 (4) (2015) 459–462.

[15] S. Novais, M.S. Ferreira, J.L. Pinto, Determination of thermo-optic coefficient of ethanol-water mixtures with optical fiber tip sensor, Opt. Fiber Technol. 45 (2018) 276–279.

[16] Y.H. Kim, S.J. Park, S.W. Jeon, S. Ju, C.S. Park, W.T. Han, B.H. Lee, Thermo-optic coefficient measurement of liquids based on simultaneous temperature and refractive index sensing capability of a two-mode fiber interferometric probe, Opt. Express 20 (21) (2012) 23744–23754.

[17] R.C. Kamikawachi, A.S. Paterno, H.J. Kalinowski, M. Muller, J.L. Pinto, J.L. Fabris, Determination of thermo-optic coefficient in liquids with fiber Bragg grating refractometer, Opt. Commun. 281 (4) (2007) 621–625.

[18] Y. Zhao, X.G. Li, L. Cai, A highly sensitive Mach–Zehnder interferometric refractive index sensor based on core-offset single mode fiber, Sens. Actuators A Phys. 223 (2015) 119–124.

[19] Y. Zhao, X.G. Li, L. Cai, Y. Yang, Refractive index sensing based on photonic crystal fiber interferometer structure with up-tapered joints, Sens. Actuators B Chem. 221 (2015) 406–410.

[20] O. Duhem, J.F. Henninot, M. Douay, Study of in fiber Mach–Zehnder interferometer based on two spaced 3-dB long period gratings surrounded by a refractive index higher than that of silica, Opt. Commun. 180 (4-6) (2000) 255–262.

Biographies

Cheng-Ling Lee received the Ph.D. degree from the Institute of Electro-Optical Engineering, National ChiaoTung University, Hsinchu, Taiwan, in 2003. During 2004–2010, she was an associate professor with the Department of Electro-Optical Engineering, National United University, Miaoli, Taiwan. In 2011, she became a full professor. Dr. Lee is the OSA memberand is the author of more than45peer reviewed publications in scientific journals.Her special fields of interests include fiber-based devices, optical fiber sensors and all-fiberinterferometers.

Yang Lu was born in 1993. He received the B.S. degree from National United University, Taiwan, in 2013. He is currently a master student with Department of Electro-Optical Engineering, National United University, Miaoli, Taiwan. His research interests include fiber based devices and optical fiber sensors.

Chien-Hsing Chen received the Ph.D. degree from the Department of Physics, National Chung Cheng University, Chiayi, Taiwan, in 2013. During 2014–2016, he was a postdoctoral fellow with the Department of Chemistry and Biochemistry and Center for Nano Bio-Detection, National Chung Cheng University, Chiayi, Taiwan.In 2018, he became anassistant research fellow with the General Research Service Center, National Pingtung University of Science and Technology, Pingtung, Taiwan. His special fields of interests include laser micro-machining techniques, optical fiber sensors and particle plasmon resonance sensors.

Chao-Tsung Ma received the B.S. degree in electrical engineering from the National Taiwan University of Science and Technology, Taipei, Taiwan, in 1989, the M.S. degree from the University of Missouri, Columbia, in 1992, and the Ph.D. degree from the University of Strathclyde, Glasgow, U.K., in 2000. His employment experiences include the R&D engineer with GeoTech, Taiwan and many years in teaching technical courses in the fields of applied power electronics and energy conversion systems. He is currently an associate professor and the head of applied power electronics systems research group (APESRG) in the department of electrical engineering, college of electrical engineering and computer science, National United University, Taiwan. His special research fields of interest include optical sensor devices, sensing technologies, applied power electronics, energy conversion and storage systems.